

## Transmission electron microscopy investigation of Ag-free lillianite and heyrovskýite from Vulcano, Aeolian Islands, Italy

DONATELLA MITOLO,<sup>1</sup> GIAN CARLO CAPITANI,<sup>2,\*</sup> ANNA GARAVELLI,<sup>1</sup> AND DANIELA PINTO<sup>1</sup>

<sup>1</sup>Dipartimento Geomineralogico, Università degli Studi di Bari, Via Orabona, 4, 70125 Bari, Italy

<sup>2</sup>Dipartimento di Scienze Geologiche e Geotecnologie, Università degli Studi di Milano “Bicocca,” P.zza della Scienza, 4, 20126 Milano, Italy

### ABSTRACT

We present a transmission electron microscopy (TEM) investigation of lillianite ( $\text{Pb}_3\text{Bi}_2\text{S}_6$ ) and heyrovskýite ( $\text{Pb}_6\text{Bi}_2\text{S}_9$ ), from Vulcano, Aeolian Islands, Italy. The minerals investigated represent the only naturally occurring Ag- and Cu-free sulfosalts in the lillianite homologous series (LHS). Three methods (crushing, ion-milling, and ultramicrotomy) were used to prepare TEM specimens. Selected area electron diffraction (SAED) patterns and high-resolution TEM (HRTEM) images indicate well-ordered crystals with only minor stacking faults and, more rarely, nanoscale intergrowths of lillianite and heyrovskýite. The latter were sometimes found to form an incommensurate structural modulation with an angle of  $\sim 29^\circ$  relative to  $\mathbf{b}^*$  in the ( $hk0$ ) plane and a wavelength of  $\sim 75 \text{ \AA}$ . This represents the first observation of such incommensurate modulations in heyrovskýite. Although considerable evidence points toward an artifact induced by the sample preparation technique (i.e., ion-milling), the possibility that the incommensurate modulation could be a primary feature of heyrovskýite itself cannot be completely ruled out. The modulation could derive from an ordering process of Pb and Bi cations over Me4 and Me5 sites within the PbS-like layer or from ordering of vacancies, naturally present or induced by  $\text{Bi}_2\text{S}_3$  sublimation during ion-milling.

**Keywords:** Lillianite, heyrovskýite, Vulcano, incommensurate modulation, TEM

### INTRODUCTION

Nearly all natural lillianite, ideally  $\text{Pb}_3\text{Bi}_2\text{S}_6$ , and heyrovskýite, ideally  $\text{Pb}_6\text{Bi}_2\text{S}_9$ , crystals contain small amounts of substitutional Ag and/or Cu in their structures (Pring et al. 1999; Pring and Etschmann 2002; Makovicky et al. 1991). Lillianite and heyrovskýite from Vulcano are, however, essentially Ag- and Cu-free members of the lillianite homologous series (LHS) (Makovicky and Karup-Møller 1977a, 1977b). Their structures are based on alternating layers of “galena-like” type cut parallel to (131) of the cubic PbS structure and stacked in a twinning relationship along [010] of LHS ( $Bbmm$  setting). Diverse members of the series differ in thickness of the “galena-like” slabs, expressed by the number ( $N$ ) of octahedra running diagonally across an individual slab of the PbS archetype and parallel to [011]<sub>PbS</sub>. Each mineral of the LHS is denoted as  $^{N1,N2}L$ , where  $N1$  and  $N2$  are the values of  $N$  for two adjacent mirror-related slabs (Makovicky 1977; Makovicky and Karup-Møller 1977a). Lillianite and heyrovskýite (Fig. 1) are, respectively, the homologues  $^{44}L$  and  $^{77}L$  of the series (Table 1).

Most studies on natural Pb- and Bi-sulfosalts (Takagi and Takéuchi 1972; Takéuchi and Takagi 1974; Makovicky et al. 1991; Pring et al. 1999; Pring and Etschmann 2002; Pring and Ciobanu 2007) or their synthetic analogues (Skowron and Tilley 1986, 1990) concern samples containing Ag and/or Cu as Pb substitutes, according to the well-known substitutional mechanism  $2\text{Pb}^{2+} = \text{Ag}(\text{Cu})^+ + \text{Bi}^{3+}$ . Price and Yeomans (1984), as well as Pring and Graeser (1994), suggested that Ag and other

monovalent cations play a role in stabilizing some polytypic structures. In particular, the distribution of Ag in the LHS structures controls the thickness of the galena-like slabs (Makovicky 1977), and this may influence the stability of the homologues (Price and Yeomans 1984; Skowron and Tilley 1990), although the reasons are not well understood.

Detailed structural investigations on natural Ag- and Cu-free lillianite and heyrovskýite have only been published in recent years (Borodaev et al. 2001, 2003; Pinto 2004; Pinto et al. 2006; Balić-Žunić et al. 2007). Each of these studies has been carried out on natural materials formed at Vulcano (Aeolian Islands, Italy), under high-temperature fumarole conditions. The absence of Ag and Cu in heyrovskýite and lillianite from Vulcano is related to the lack of these monovalent cations in the fumarole fluids from which the crystals formed (Borodaev et al. 2001, 2003).

HRTEM has been widely used in structural and microstructural investigations on oxide and silicate minerals. In contrast, there are relatively few HRTEM studies on sulfides-sulfosalts (i.e., Pierce and Buseck 1978; Akizuki 1981, 1983; Kissin and Owens 1986; Williams and Hyde 1988; Williams and Pring 1988; Pring 1989, 1990, 1995, 2001; Pring and Hyde 1987; Pring et al. 1993; Pring and Graeser 1994; Ciobanu et al. 2004). Even fewer HRTEM studies on LHS compounds have been reported in the literature, including those on natural minerals (Pring et al. 1999; Pring and Etschmann 2002; Pring and Ciobanu 2007) or their synthetic analogues (Prodan et al. 1982; Tilley and Wright 1982; Skowron and Tilley 1986, 1990).

TEM investigations on synthetic analogues of LHS date back to the studies of Tilley and Wright (1982) and Prodan et al. (1982). These studies showed that lillianite and heyrovskýite are

\* E-mail: giancarlo.capitani@unimib.it

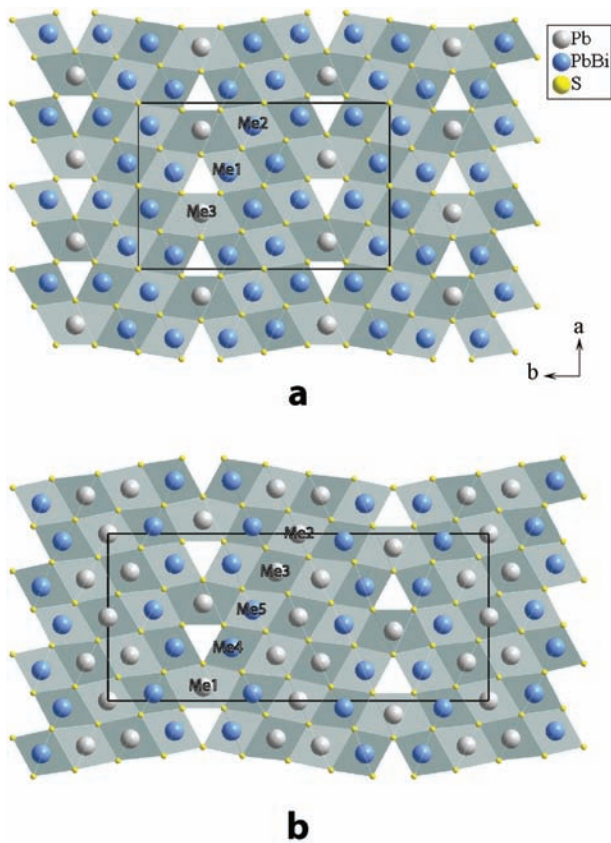


**FIGURE 1.** Structural projections of lillianite (a) and heyrovskýite (b) down [001] [*Bbmm* setting; after Makovicky (1977) and Takeuchi and Takagi (1974), respectively; site occupancy in lillianite is modified after Pinto et al. (2006)]. Shaded areas represent Pb and Pb/Bi polyhedra. Bright and dark polyhedra represent different heights along [001].

the only stable ternary phases in the PbS-rich region of the PbS-Bi<sub>2</sub>S<sub>3</sub> system. The coexistence of heyrovskýite with galena and the coherent intergrowth of heyrovskýite and lillianite suggest that additional ordered phases with intermediate compositions are unlikely to form. In contrast, in their HRTEM studies of quenched and annealed materials in the PbS-rich region of the PbS-Bi<sub>2</sub>S<sub>3</sub>-Ag<sub>2</sub>S system, Skowron and Tilley (1990) found a large variety of ordered phases of LHS homologues, including <sup>4,5</sup>L, <sup>7,8</sup>L, and <sup>8,8</sup>L (not yet found in nature), as well as disordered phases and ordered sequences. These authors observed that homologues with *N* = 4 or 7 blocks, either ordered or disordered, were dominant

phases at 700 °C, whereas a wide variety of homologues occurred at 500 °C. Besides the proliferation of LHS phases, the addition of Ag<sub>2</sub>S component to the PbS-Bi<sub>2</sub>S<sub>3</sub> system was claimed to stabilize slabs of galena-like structural units that are five- and eight-octahedra in width. All these studies on synthetic LHS materials reported also about electron beam damage of sulfosalts. The loss of crystallinity may result from Bi<sub>2</sub>S<sub>3</sub> sublimation due to sample heating under prolonged electron beam exposure or transformation of the chemically twinned phases to galena under electron beam irradiation (Skowron and Tilley 1986).

HRTEM studies on natural samples have focused on Ag-bearing LHS minerals from the Ivigtut cryolite deposit, South Greenland. Pring et al. (1999) described extensive regions of disordered intergrowths of lillianite/gustavite-like (*N* = 4) and heyrovskýite-like (*N* = 7) blocks. In one case, oscillating Pb/Bi concentration was inferred from the observed distribution of blocks with *N* = 4 and *N* = 7. A compositional fluctuation on the order of 70–170 Å over a region of 1800 Å long, including a 220 Å lamella of ordered vikingite, which yielded an average homologue number *N* = 4.92, was observed. The relative stability among well-ordered phases (vikingite and gustavite), longer ordered sequences (e.g., 4,4,4,7, 7,7,7,4, etc.), and disordered sequences was established to decrease in this order. Long period ordered intergrowths were thus interpreted as an intermediate stage of a diffusion-controlled exsolution process from a heterogeneous, unknown precursor with *N*<sub>aver</sub> ~5 that could evolve into ordered vikingite and gustavite. Pring and Etschmann (2002) described coherent intergrowths of Cu- and Ag-rich cosalite (Cu<sub>1.2</sub>Ag<sub>0.9</sub>Pb<sub>6.7</sub>Bi<sub>8.3</sub>S<sub>20</sub>) with members of the lillianite-gustavite series (Pb<sub>3</sub>Bi<sub>2</sub>S<sub>6</sub>-PbAgBi<sub>3</sub>S<sub>6</sub>). These authors also observed a complex fringe texture in Ag-bearing cosalite and explained it as a compositional-displacive modulation related to coupled Ag/Pb/Bi and Cu/□ ordering. More recently, Pring and Ciobanu (2007) examined a crystal of eskimoite, a <sup>5,9</sup>L homologue and Ag-substituted polymorph of <sup>7,7</sup>L heyrovskýite (Table 1). They found numerous 5,5 and 9,9 “block-width errors” over a crystal edge of about 80 000 Å, but relatively minor compositional oscillations since 5,5 and 9,9 blocks occurred closely spaced and the average homologue number *N* = 7.07 was very close to that of stoichiometric eskimoite. Nevertheless, they deduced a medium-range (100–150 Å) compositional oscillation in Ag within the longer-range modulation.

In this work, we report the first TEM investigation of lillianite and heyrovskýite from Vulcano. The results include a description of the microstructures found in these Cu- and Ag-free sulfosalts compared with those that occur in natural Ag- and Cu-bearing

**TABLE 1.** Compositional and structural data for selected sulfosalts of the lillianite homologous series (from Ferraris et al. 2004, modified)

Mineral	Formula	LHS	<i>a</i> (Å)	<i>b</i>	<i>c</i>	<i>α</i> (°)	<i>β</i>	<i>γ</i>	Space group
Lillianite	Pb <sub>3</sub> Bi <sub>2</sub> S <sub>6</sub>	<sup>4,4</sup> L	13.54	20.45	4.10	–	–	–	<i>Bbmm</i>
Xilingolite	Pb <sub>3</sub> Bi <sub>2</sub> S <sub>6</sub>	<sup>4,4</sup> L	13.51	4.09	20.65	–	92.2	–	<i>C2/m</i>
Gustavite	PbAgBi <sub>3</sub> S <sub>6</sub>	<sup>4,4</sup> L	7.08	19.57	8.27	–	107.2	–	<i>P2<sub>1</sub>/c</i>
Vikingite	Pb <sub>8</sub> Ag <sub>5</sub> Bi <sub>13</sub> S <sub>30</sub>	<sup>4,7</sup> L	7.10	8.22	25.25	90	95.36	106.8	<i>P1</i>
Ramdohrite	Pb <sub>6</sub> Sb <sub>11</sub> Ag <sub>3</sub> S <sub>24</sub>	<sup>4,4</sup> L	19.24	13.08	8.73	–	90.3	–	<i>P2<sub>1</sub>/n</i>
Andorite IV	Pb <sub>18</sub> Ag <sub>15</sub> Sb <sub>47</sub> S <sub>96</sub>	<sup>4,4</sup> L	13.04	19.18	17.07	–	–	90	<i>P2<sub>1</sub>/a</i>
Andorite VI	PbAgSb <sub>3</sub> S <sub>6</sub>	<sup>4,4</sup> L	13.02	19.18	25.48	–	–	–	<i>Pn2<sub>1</sub>/a</i>
Heyrovskýite	Pb <sub>6</sub> Bi <sub>2</sub> S <sub>9</sub>	<sup>7,7</sup> L	13.71	31.21	4.13	–	–	–	<i>Bbmm</i>
Aschamalmite	Pb <sub>5.92</sub> Bi <sub>2.06</sub> S <sub>9</sub>	<sup>7,7</sup> L	13.71	4.09	31.43	–	91	–	<i>C2/m</i>
Ag-Bi-heyrovskýite	Pb <sub>3.36</sub> Ag <sub>1.32</sub> Bi <sub>3.32</sub> S <sub>9</sub>	<sup>7,7</sup> L	4.11	13.60	30.49	–	–	–	<i>Cmcm</i>
Eskimoite	Ag <sub>7</sub> Pb <sub>10</sub> Bi <sub>15</sub> S <sub>36</sub>	<sup>5,9</sup> L	13.46	30.19	4.10	–	93.4	–	<i>B2/m</i>
Ourayite	Pb <sub>4</sub> Ag <sub>3</sub> Bi <sub>5</sub> S <sub>13</sub>	<sup>11,11</sup> L	13.49	44.17	4.05	–	–	–	<i>Bbmm</i>

phases and their synthetic analogues. Because of the high sensitivity of sulfosalts to focused beams (see also Loginov and Brown 1992), results are also discussed with respect to TEM specimen preparation techniques employed (i.e., ion-milling vs. ultramicrotomy) and to observation conditions (electron dose). In this frame, for the first time, we describe an incommensurate structural modulation in heyrovskýite, although its origin remains unclear.

## EXPERIMENTAL METHODS

### Samples

The minute, lead-gray crystals of sulfosalts used in this study were collected from deep walls of a fumarole vent located on the northern inner slope of the La Fossa crater of the Vulcano island (fumarole IC,  $T = 400\text{--}460\text{ }^{\circ}\text{C}$ ). From a morphological point of view, lillianite and heyrovskýite are very similar and cannot be distinguished even with the aid of an optical microscope. Both sulfosalts occur either as needle-like crystals, up to  $300\text{ }\mu\text{m}$  in length and  $70\text{ }\mu\text{m}$  in width, or larger lath-like crystals, both silvery gray in color and with a metallic luster. Several fragments of the crystals were hand picked, and their compositions were verified by energy dispersive X-ray (EDX) spectrometry on a scanning electron microscope (SEM).

Electron microprobe and single-crystal XRD analyses of several fragments from the same suite of crystals have been performed in previous studies (Balić-Žunić et al. 2007; Mitolo 2008; Pinto et al. in review). Both Ag-free lillianite and Ag-free heyrovskýite crystals adopt the space group *Bbmm* and are homogeneous in composition, with  $N_{\text{chem}}$  (defined as the  $N$  resulting from the chemical formula) ranging from 3.896 to 4.01 and from 6.56 to 6.84, respectively. The average composition of lillianite is  $\text{Pb}_{3.02}\text{Bi}_{2.03}(\text{S}_{3.70}\text{Se}_{0.26})_{55.96}$  (mean of six point analyses), and its unit-cell parameters are  $a = 13.593$ ,  $b = 20.661$ ,  $c = 4.127\text{ }\text{Å}$ , and  $V = 1158.57\text{ }\text{Å}^3$ . The composition of heyrovskýite is  $(\text{Pb}_{5.86}\text{Cd}_{0.03})_{25.89}\text{Bi}_{2.04}(\text{S}_{8.55}\text{Se}_{0.53}\text{Cl}_{0.03})_{29.08}$  (mean of five point analyses), and its cell parameters are  $a = 13.7498(4)$ ,  $b = 31.5053(1)$ ,  $c = 4.1475(1)\text{ }\text{Å}$ , and  $V = 1796.66(7)\text{ }\text{Å}^3$ .

### TEM specimen preparation

TEM specimens of lillianite and heyrovskýite were prepared using three different methods: crushing, ion-milling, and ultramicrotomy. Crushing is the simplest and most common method. However, with this technique, crystals with pronounced anisotropy tend to settle with their cleavage faces parallel to the TEM grid, preventing observation of crystals along directions parallel to the cleavage planes. A few selected crystals were powdered in an agate mortar under ethanol to dissipate heat and reduce grinding stress of sample grains. A drop of the resultant suspension was deposited and left to dry on a carbon-coated copper grid. Since the examined crystals have (100) plate shapes, with the exception of one case, we could observe the crushed samples only along or close to their  $a$  axis.

Ion-milling has been widely used for preparation of large, electron transparent TEM specimens. [001] pre-oriented crystal fragments were glued on a side of a microscope cover glass ( $2 \times 1 \times 0.17\text{ mm}$ ), mounted onto a copper ring, and then thinned down to electron transparency with a Gatan Precision Ion-Polishing System (PIPS). The operating voltages of PIPS were 3–5 keV, and the beam incidence to the sample surface was  $\pm 10^{\circ}$ . The recovered TEM mounts were then carbon-coated to avoid electrostatic charging during TEM observation. However, ion milling may induce artifacts due to preferential sputtering, sample heating, and radiation damage (Barber 1970). For our specimens, it seems that sample heating may have induced partial sublimation of sulfosalts. This prompted us to employ an alternative sample preparation technique, i.e., ultramicrotomy.

Ultramicrotomy is a technique widely employed in life sciences to cut soft biological samples into thin cross-sections ( $<100\text{ nm}$ ). In mineralogy, the use of this technique is relatively rare, largely because minerals are in general hard to cut. According to Malis and Steele (1990), who applied ultramicrotomy to several crystalline materials, only small wedges of electron-transparent areas, accompanied by crushed and strained regions, could be obtained. Nevertheless, successful application of this method has been reported for muscovite (e.g., Amouric and Baronnet 1983), and we have tried it on sulfosalts, which possess slightly higher but still relatively low hardness (2–2.5 vs. 2–4, respectively). Our motivation to use ultramicrotomy was to rule out the possibility of any artifacts induced by ion-milling, while maintaining the advantage of observing the lillianite and heyrovskýite crystals along  $c$ . Several crystals were embedded in a low viscosity epoxy resin

(“Spurr resin,” Spurr 1969) and were cut along their (001) planes (perpendicular to  $c$ ) with an Ultracut ultramicrotome. The recovered slices, 40–50 nm in thickness, were mounted on formvar-coated copper grids and were then carbon coated.

## TEM OBSERVATIONS

Sulfosalt specimens were analyzed at the Dipartimento Geomineralogico of the University of Bari with a JEOL JEM 2010 electron microscope operating at 200 keV with a LaB<sub>6</sub> electron source, equipped with an EDX detector and a  $\pm 20^{\circ}$  double-tilt specimen holder. The spherical aberration ( $C_s$ ) of the TEM is 0.5 mm, and its theoretical point-to-point resolution is 1.94 Å.

Digital images were acquired on a Gatan MSC794 CCD. To remove the noisy contrast from the amorphous material, HRTEM images were ABS-filtered (Average Background Subtraction, Kilaas 1998) with an HRTEM filter (Mitchell 2007), as implemented in Gatan Digital Micrograph (version 3.9). When required, additional Fourier filtering was applied using the masking tools in program CRISP (Hovmöller 1992). HRTEM image simulations were performed with NCEMSS v. 1.8 (Kilaas 1998).

## RESULTS

### Lillianite and lillianite-heyrovskýite intergrowths

Typically, the lillianite and heyrovskýite crystals investigated exhibit a well-ordered microstructure free of major defects. SAED patterns could be easily attributed to either lillianite or heyrovskýite, and were free of streaks and extra spots, indicating the absence of intergrowths. Lillianite was recognized on [001] diffraction patterns by the correspondence of the strong  $311_{\text{PbS}}$  subcell reflection with 0,12,0, which results in a repeat distance along  $b$  of  $\sim 20.7\text{ }\text{Å}$  (Fig. 2). Heyrovskýite was identified by the correspondence of  $311_{\text{PbS}}$  with 0,18,0, with a repeat distance along  $b$  of  $\sim 31.3\text{ }\text{Å}$ .

Because of the significant noise affecting HRTEM images, the interpretation of the contrast on the (001) projection is not straightforward. Better information was captured on ABS-filtered images. In this case, the fish-bone features typical of the LHS chemical twinning could be recognized. Lillianite shows equally spaced (010) lattice fringes over wide areas and appears as a discrete phase with 4,4 ordered sequences of galena-like slabs (Fig. 3).

No observation-induced structural defects and/or dynamic processes, as formation of other phases or chemical reactions, were detected during our TEM investigation. However, the contrast on HRTEM images was often blurred by an inelastic signal, probably due to an amorphous film produced by ion milling and/or sample radiation damage, as mentioned above, that had to be filtered out in the frequency domain to improve the image quality.

In a few cases, stacking faults and lillianite-heyrovskýite intergrowths were observed. Similar defects are quite common in natural Ag-bearing LHS minerals (Makovicky et al. 1991; Pring et al. 1999; Pring and Etschmann 2002) and synthetic analogues (Prodan et al. 1982; Tilley and Wright 1982; Skowron and Tilley 1986, 1990). Sets of planar faults, imaged as dark and bright straight lines, were observed once in an ordered matrix of lillianite (Fig. 4), but their nature could not be determined because the sample was too thick. In a second case, a  $\sim 145\text{ }\text{Å}$  wide strip of heyrovskýite was observed within the lillianite (Fig. 5a). The regular order of lillianite was also altered by the presence of a single lamella having a periodicity of  $\sim 24\text{ }\text{Å}$ . This lamella is consistent with cosalite,  $\text{Pb}_2\text{Bi}_2\text{S}_5$ . However, it is more likely to be vikingite, which has a  $4^7\text{L}$  structure with

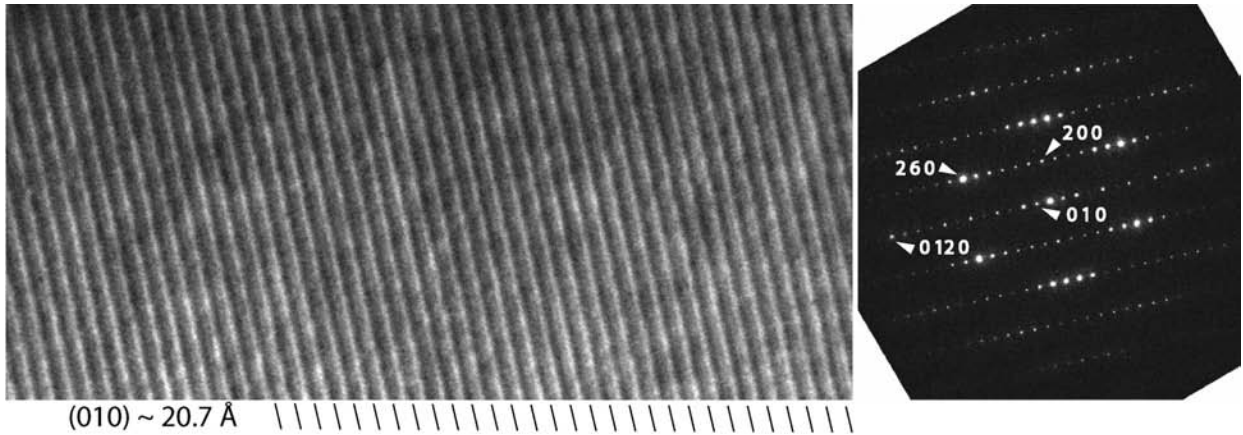


**FIGURE 2.** (a) Image of lattice fringes of lillianite taken down [001]. Note the ordering sequence of equally spaced (010) lattice fringes with an interplanar distance of about 20.7 Å. (b) Selected area electron diffraction (SAED) pattern of lillianite. Note the absence of streaks and extra spots.

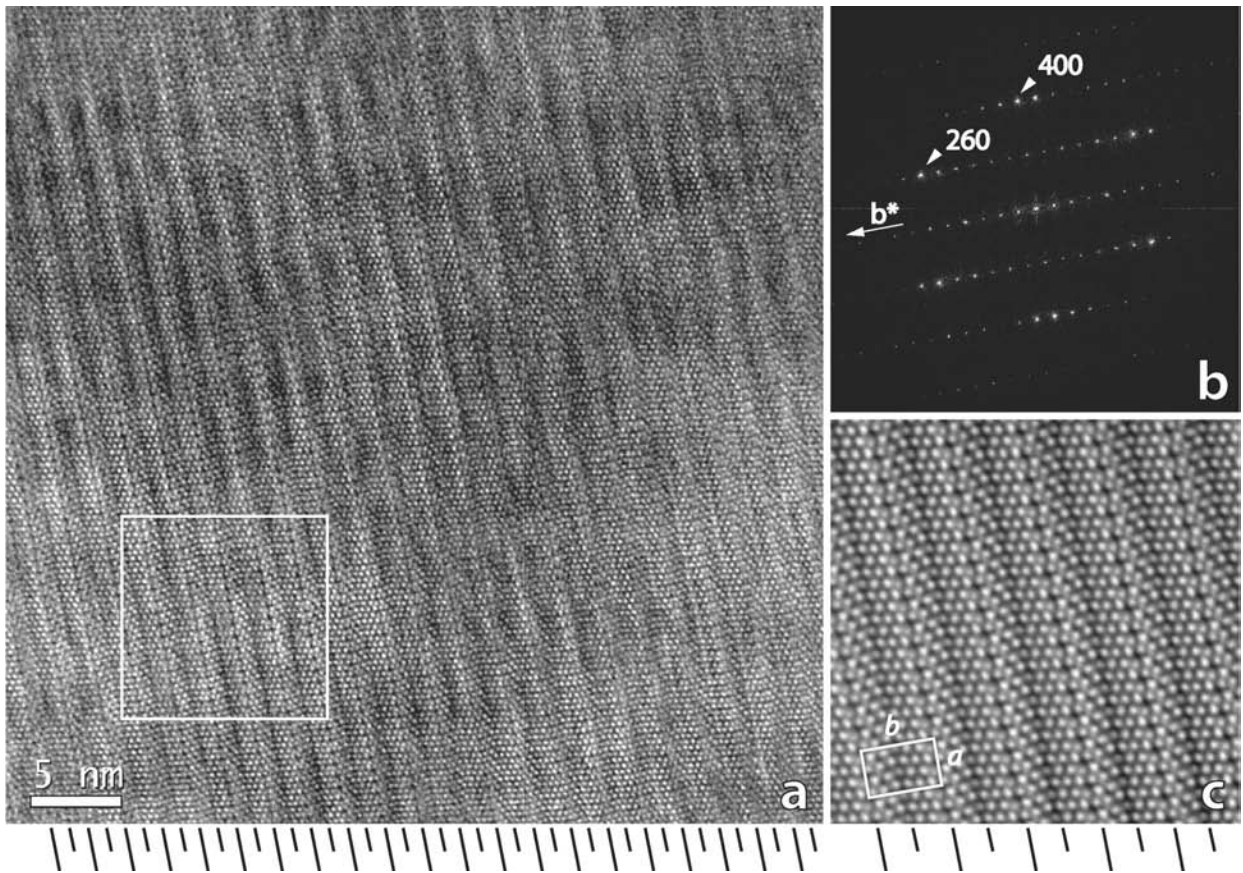


**FIGURE 3.** (a) ABS-filtered HRTEM image of lillianite taken down [001]. Note the ordering sequence of equally spaced (010) lattice fringes (long lines) and twin planes (short lines). (b) Fast Fourier transform (FFT) of a with some sublattice PbS reflections indicated. (c) Fourier filtered image of the square area indicated in a. The projected unit cell of lillianite is outlined. Note the symmetrical fish-bone structure typical of 4,4 lillianite.

a  $\sim 25$  Å repeat, since cosalite is not a LHS homologue (Table 1). Nevertheless, cosalite-lillianite lamellar intergrowths were reported by Pring and Etschmann (2002), in a natural sample from Ivigtut (Greenland). In addition, a single lamella  $\sim 37$  Å wide was also observed within heyrovskýite. Such a repeat is

consistent with a single lamella of mozgovaite,  $\text{PbBi}_4(\text{S,Se})_7$  (Vurro et al. 1999), intergrown with heyrovskýite, but for the same reason described above it is probably a 9,9 LHS, which has approximately the same width.

The lillianite-heyrovskýite boundary is also affected by

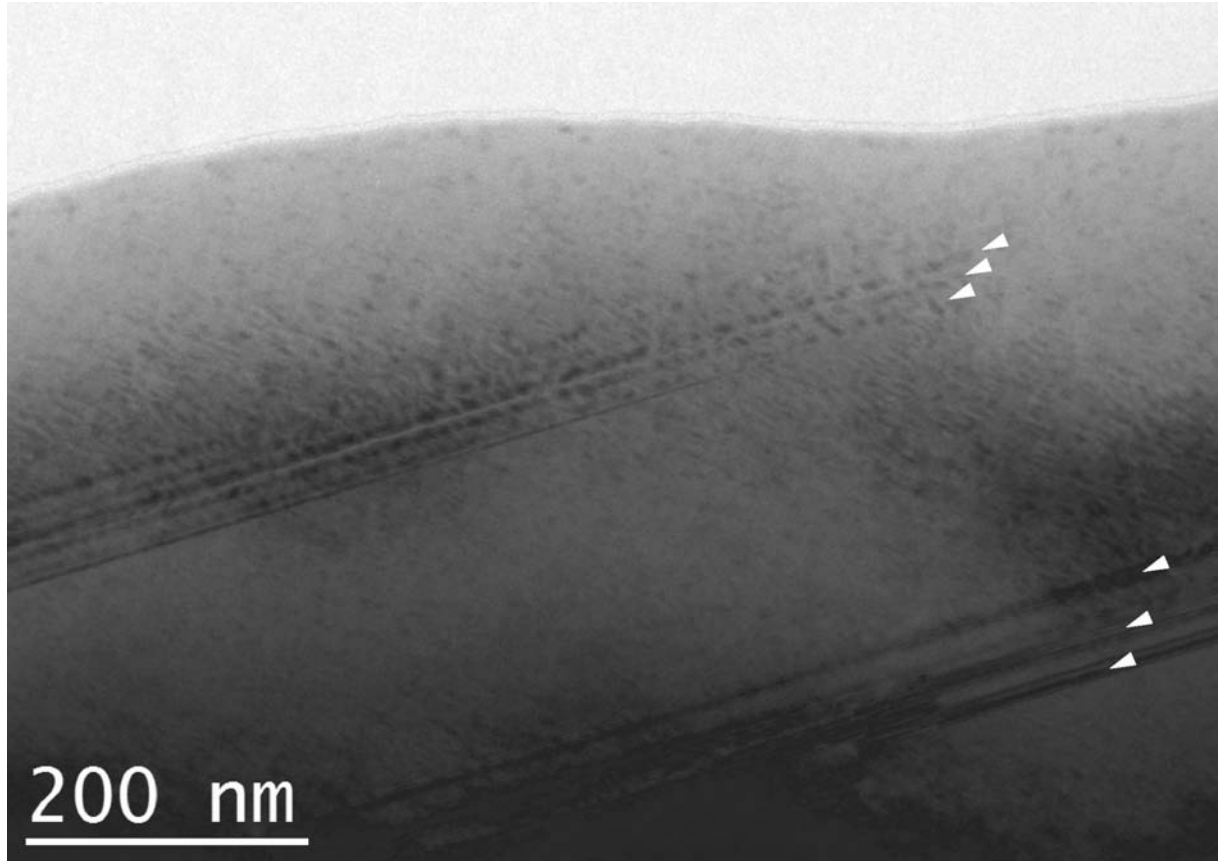


FIGURE 4. Bright-field (BF) image of lillianite containing stacking faults (arrowed).

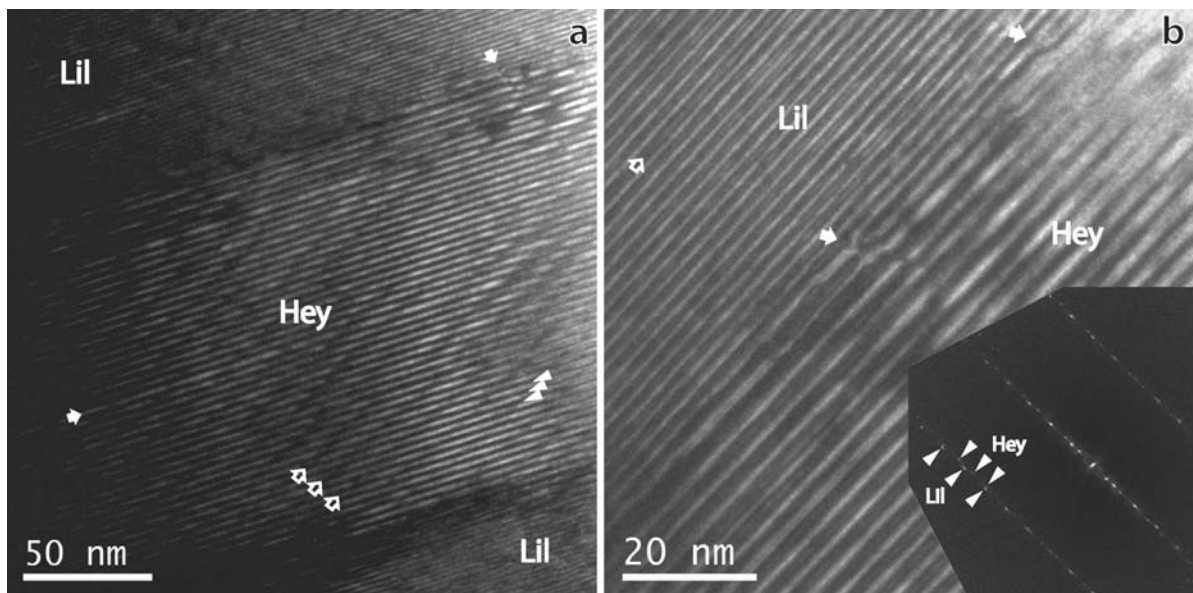


FIGURE 5. (a) Heyrovskýite lamella within lillianite. Note that the dark bands of the incommensurate modulation (large empty arrows) cross-cut (010) lattice fringes (small filled arrows) of heyrovskýite. Note also a single lamella,  $\sim 37$  Å wide, consistent with mozgovaite or 9,9 LHS, within heyrovskýite. (b) Lillianite-heyrovskýite interface. Filled arrows indicate dislocation-like features. This defective microstructure probably arises from slight crystallographic misorientation between the two intergrown phases, as reflected by the FFT taken across the interface (inset), rather than lack of coherence along (010). A lamella,  $\sim 24$  Å wide, consistent with cosalite or vikingite, within lillianite, is indicated by an empty arrow.

several dislocation-like microstructural features [see edge-on in [001] HR images (Fig. 5b)], which connect sulfosalts lamellae of different widths along the *a*-axis. This defective microstructure is probably a growth feature indicative of an only partially coherent lillianite/heyrovskýite interface. Lack of complete coherence may be due to a slightly different crystallographic orientation between lillianite and heyrovskýite, rather than incommensurability on (010), as suggested by the small misalignment between  $[hk0]^*$  rows in the FFT taken across the lillianite-heyrovskýite boundary (Fig. 5b, inset). Defects with a similar appearance were described by Skowron and Tilley (1986) and Pring et al. (1999). The authors considered these defects as “block-width defects” since they are associated, for instance, with the change from a 4,4 gustavite plus a 7,7 heyrovskýite sequence to 4,7 vikingite.

### Heyrovskýite incommensurate modulations

Surprisingly, heyrovskýite crystals prepared by ion-milling show incommensurate structural modulations. In reciprocal space, weak satellite reflections were observed on (*hk*0) planes, making an angle of  $\sim 29^\circ$  with  $\mathbf{b}^*$  with an average wavelength

of  $\sim 75 \text{ \AA}$  (Fig. 6). In direct space, the incommensurate modulation was best imaged in diffraction contrast images as broad fringes crosscutting the (010) fringes (Fig. 7). Depending on the exact diffracting condition, a single modulation or a system of two symmetrically related modulations, which form a kind of tweed pattern, were observable (Fig. 8). The incommensurate modulation could also be seen on HRTEM images (Fig. 9). The possibility that the modulation contrast might represent moiré fringes due to partings of the crystal on (001) and rotation of the crystal lattice around [001] (the direction of the electron beam), was considered. According to the relation  $d_m = d_{010}/[2 \cdot \sin(\beta/2)]$  (Williams and Carter 1996), where  $d_m$  is the observed modulation spacing (75 Å) and  $d_{010}$  is the periodicity of the (010) planes (31.5 Å), the observed features could be reproduced by a second crystal rotated by an angle ( $\beta$ ) of  $\sim 24^\circ$  around [001] with respect to the primary crystal. However, no diffraction effects associated with this hypothetical second crystal (or any other phase) were ever observed in heyrovskýite crystals that showed modulations. Moreover, the fact that no higher harmonics are detectable in our SAED patterns may merely signify that the modulation

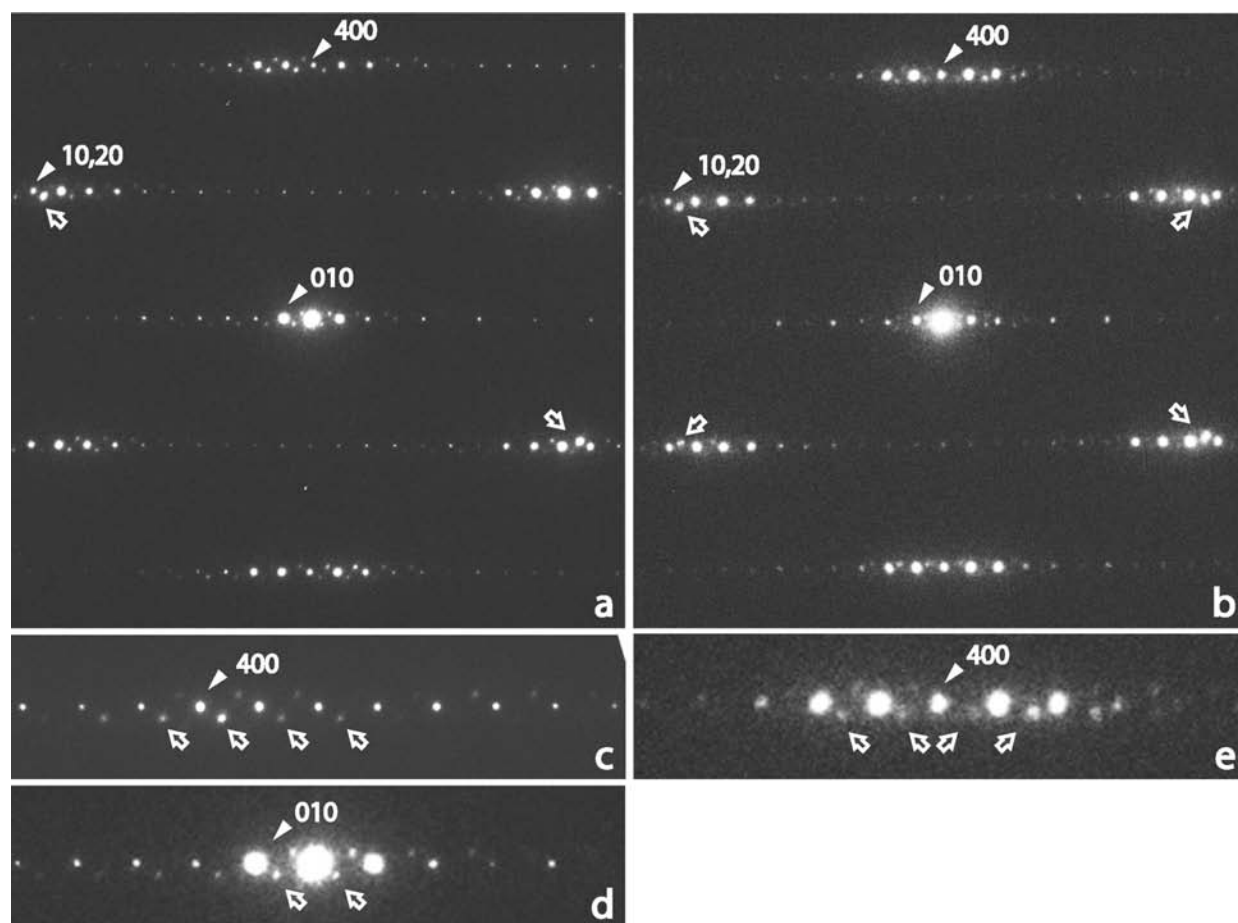


**FIGURE 6.** SAED pattern of heyrovskýite down [001]. Depending on the exact diffracting conditions, one system of modulation (a) or two mirror-related systems (b) could be excited. These, in turn, gave rise to the bright field images of Figures 7 and 8, respectively. Enlarged portions of the reciprocal space around the 400 diffracted spot (c) and the transmitted beam (d) of a. (e) Enlarged portion of the reciprocal space around the 400 diffracted spot of b. Satellite reflections of the incommensurate modulation are indicated by empty arrows and heyrovskýite reflections by the small filled arrows.

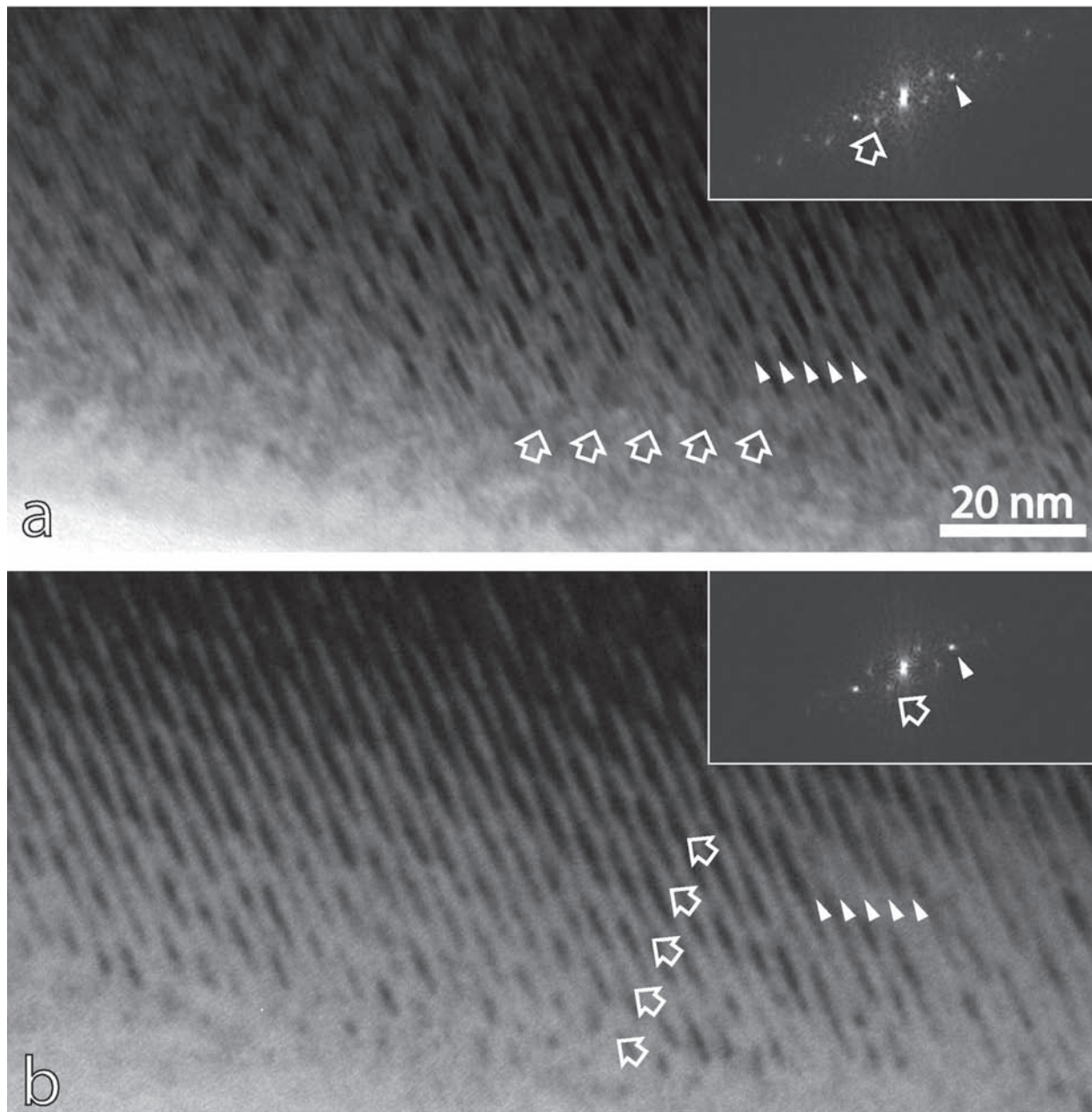


**FIGURE 7.** Lattice fringes images of heyrovskýite close to the [001] zone. Depending on the direction of departure from the exact diffraction condition, (a) one system of incommensurate modulation or (b) the other system could be imaged (empty arrows). Note that both systems cross-cut the lattice fringes (small filled arrows) at approximately the same angle. Note the geometrical relationship between the two systems in FFTs (insets).

is purely sinusoidal.

It should be noted that modulations were already present at the very first instant of beam illumination, and so it is unlikely that they were produced by exposure to the electron-beam. Moreover, modulations were observed in heyrovskýite but not in lillianite crystals present in the same TEM specimen. Even in heyrovskýite-lillianite intergrowths, modulations were clearly visible in heyrovskýite but only barely perceivable in lillianite in contact with heyrovskýite (supposedly mechanically induced) and absent far from the contact (Fig. 5a). One

may wonder why such structurally and compositionally similar phases, which experienced the same beam dose during preparation and observation, behaved so differently. Such incommensurate modulations have not been reported before in natural Ag-bearing LHS homologues (Makovicky et al. 1991; Pring et al. 1999), or their synthetic analogues (Prodan et al. 1982; Tilley and Wright 1982; Skowron and Tilley 1986, 1990). However, displacive structural modulations occur in sartorite ( $\text{PbAs}_2\text{S}_4$ ) (Pring et al. 1993), and a compositional and displacive modulation has been described for a cosalite

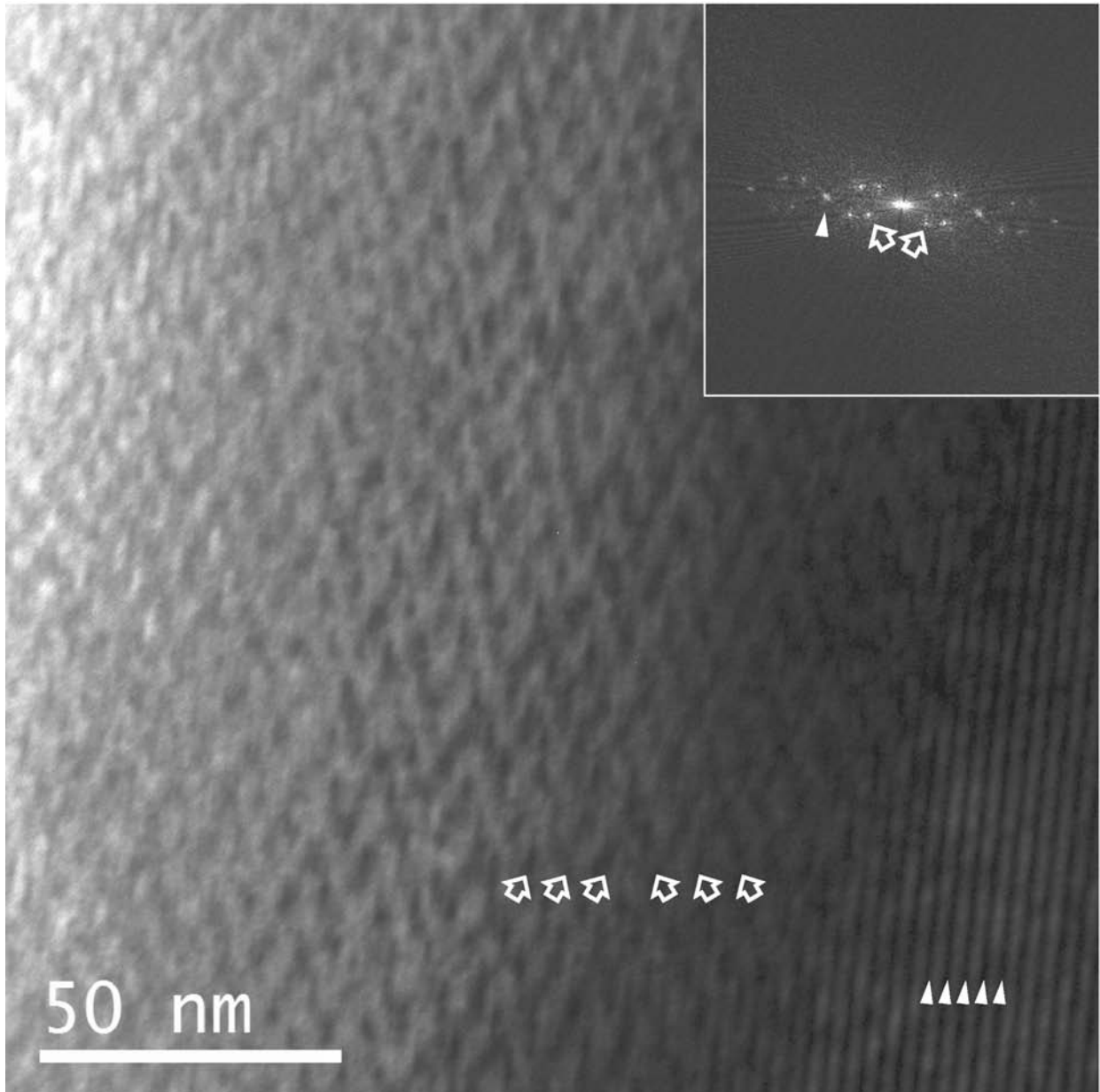


**FIGURE 8.** Lattice fringes image of heyrovskýite down [001] in which both systems of the incommensurate modulations are equally excited and appear as a tweed-like microstructure. Accordingly, the FFT (inset) shows two systems of satellite reflections (symbols as in Fig. 7).

sample from Ivigtut (Pring and Etschmann 2002).

To investigate the origin of the structural modulation, i.e., to distinguish between “primary” features and “artifacts” induced by specimen preparation, additional specimens of the same material were prepared by ultramicrotomy. No incommensurate structural modulations were observed in ultramicrotomed sulfosalts. Moreover, the contrast in these samples is much clearer, i.e., the inelastic scattering is much lower than that in ion-milled samples (Fig. 10). The heyrovskýite 7,7 ordered sequences of galena-like slabs can now be distinguished in HRTEM images (Fig. 11). The contrast is dominated by wavy rows of brighter dots that can be matched with sulfur atom posi-

tions that outline the Pb, Pb/Bi octahedral sites and bicapped trigonal-prismatic sites at mirror planes (Fig. 12).

As an additional verification, a needle-like crystal of natural Ag-free heyrovskýite,  $450 \times 54 \times 13 \mu\text{m}$ , was investigated by single-crystal X-ray diffraction at the ELETTRA synchrotron facility. The use of synchrotron radiation is justified by the high brilliance of the synchrotron source, which in principle should allow the detection of weak satellite reflections. To avoid overlapping of reflections, the crystal-to-detector distance was fixed at 90 mm during the measurement. However, no trace of satellite reflections ascribable to the incommensurate modulation described above was found.

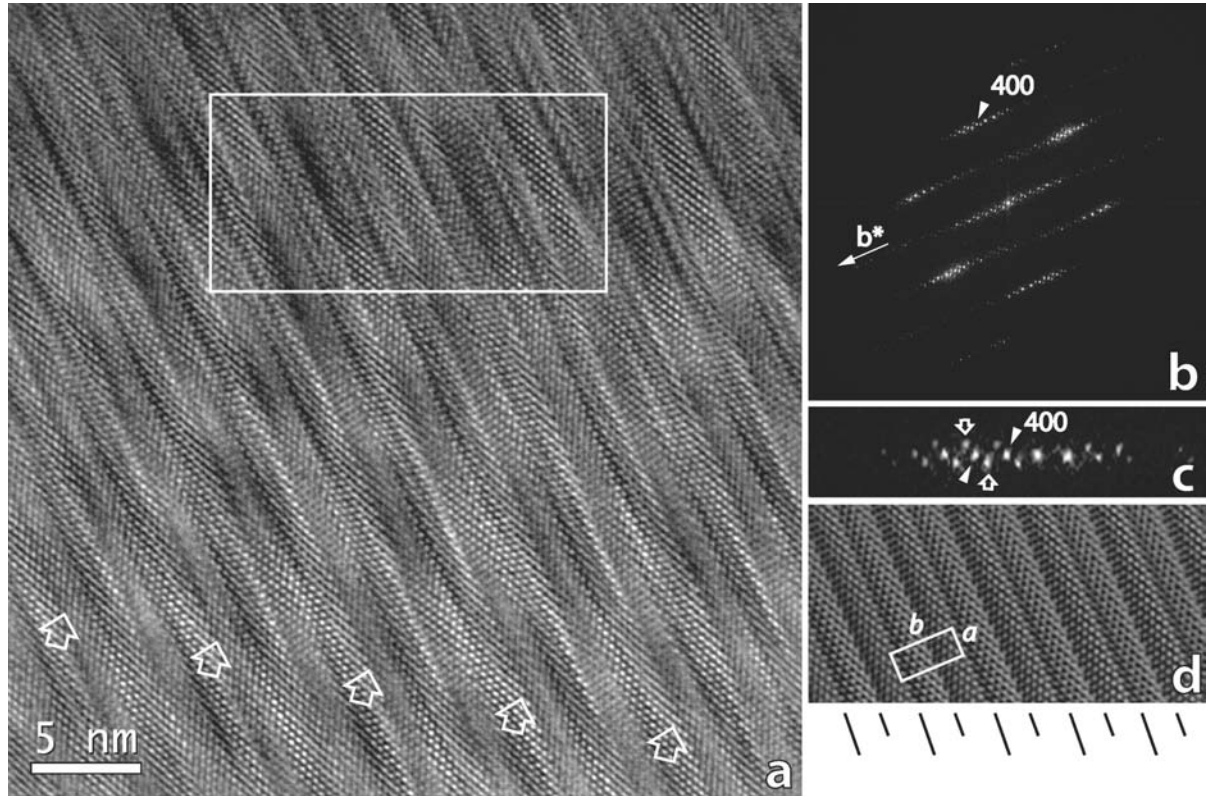


**FIGURE 9.** (a) ABS-filtered HRTEM image of heyrovskýite down [001]. Note dark bands (arrowed) cross-cut (010) lattice fringes. (b) FFT of a, and (c) an enlarged portion of the reciprocal space around the **400** spot. Note the satellite reflections of the incommensurate modulation (large empty arrows) around the strong subcell reflections (small filled arrows). (d) Fourier-filtered image of the rectangular area in a masking contributions of the incommensurate modulation and residual diffuse scattering. A symmetrical fish-bone structure typical of 7,7 heyrovskýite now can be recognized. Detailed interpretation of this image is difficult, as the crystal was slightly tilted with respect to the optimal illumination condition (see b).

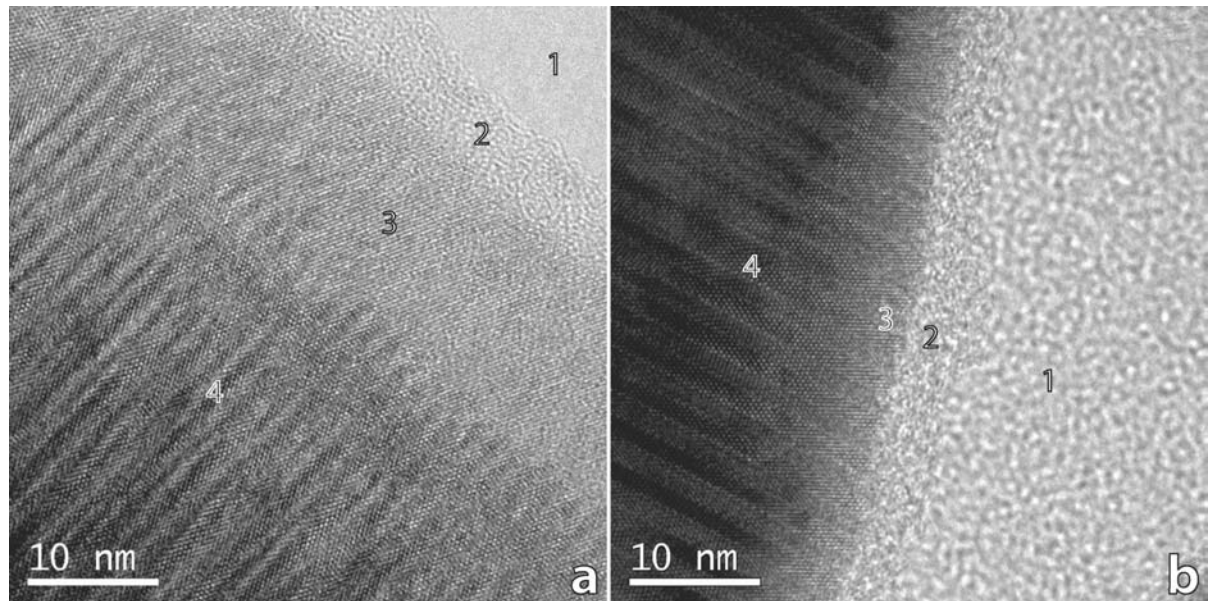


**FIGURE 10.** As-acquired HRTEM images of heyrovskýite down [001]. (a) Ion-milled specimen: 1 = void; 2 = amorphous rim; 3 = thin, poorly scattering region; 4 = damaged region. (b) Ultramicrotomed specimen: 1 = embedding resin; 2 = narrow area where the resin was detached from the specimen; 3 = thin, poorly scattering region; 4 = well-scattering region.

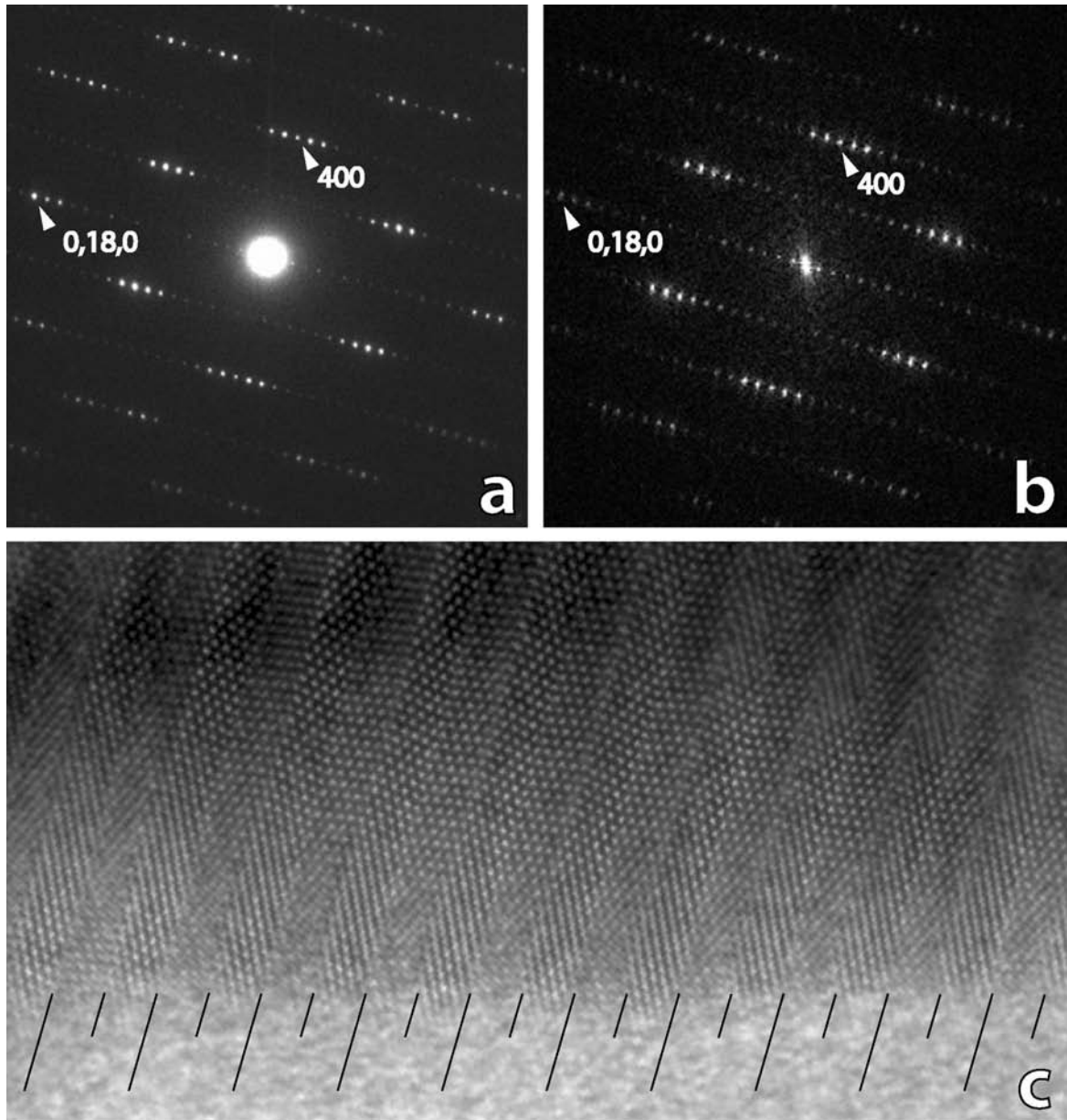


**FIGURE 11.** Ultramicrotomed heyrovskýite. (a) [001] SAED pattern. (b) FFT of the well-ordered region in Figure 10b. Note the absence of incommensurate modulation reflections in **a** and **b**. (c) ABS-filtered portion of Figure 10b. The (010) cell edges with a distance of  $\sim 31.5$  Å and the twin planes halfway are indicated by long and short lines, respectively.

## DISCUSSION

### Departing microstructure

The investigated lillianite and heyrovskýite appear, generally, as discrete phases, showing a perfectly ordered structure, with minor stacking faults and/or dislocations. In contrast, natural Ag-bearing sulfosalts are much more defective, showing a high density of stacking faults and intergrowths of different homologues (Pring et al. 1999; Pring and Etschmann 2002; Pring and Ciobanu 2007). It seems that the absence of Ag and/or Cu impurities in the Pb-Bi-S system enhances the energy barrier

between the stability fields of different homologues, allowing growth of more homogeneous crystals. Silver and Cu therefore, through their different chemical bonding, may promote polytypic disorder in the lillianite homologue series.

In a recent electron microprobe study on heyrovskýite from Vulcano, Borodaev et al. (2003) suggested the existence of several “heyrovskýites” with  $N_{\text{chem}}$  values substantially different from the ideal value  $N = 7$  ( $N \sim 5$  or  $N \sim 6$ ). However, our TEM investigation revealed no evidence of such “sub-phases” in the studied sulfosalts. Thus, it is probable that lillianite/heyrovskýite intergrowths such as those described above, which are at a scale

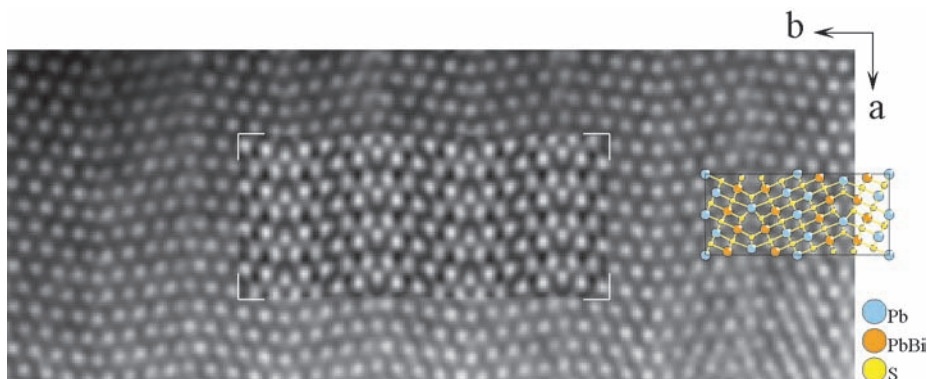


**FIGURE 12.** Experimental and calculated (inset) HRTEM images of heyrovskýite along [001]. The contrast is dominated by sulfur positions (bright dots). The calculated image was simulated using a sample thickness of 40 Å and a defocus value of  $-200$  Å. The structure of heyrovskýite (Takeuchi and Takagi 1974) is also shown for comparison.

smaller (few nanometers) than the spatial resolution of any electron microprobe for chemical analyses (few micrometers), could be the origin of these exotic values of  $N_{\text{chem}}$ .

### Incommensurate modulations

Interestingly, heyrovskýite crystals prepared by ion-milling show incommensurate structural modulations, while lillianite crystals do not. This structural modulation may be: (1) naturally present; (2) induced by ion-milling; or (3) induced by electron beam irradiation. As described above, heyrovskýite samples prepared by crushing or ultramicrotomy did not show incommensurate modulations, and neither did the single crystal used for synchrotron XRD measurement. This strongly suggests that incommensurate modulations are not produced by electron-beam irradiation and that they do not occur as primary features. Thus, these incommensurate modulations could most probably be artifacts induced by ion-milling. The elevated temperatures locally reached in the sample while being heavily irradiated by energetic  $\text{Ar}^+$  ions, coupled with high-vacuum conditions, could have induced sublimation with loss of  $\text{Bi}_2\text{S}_3$ . Since  $\text{Bi}_2\text{S}_3$  has a lower melting point than  $\text{PbS}$  [763 vs. 1110 °C, respectively, as reported by Madelung et al. (1998a, 1998b)], this sublimation process may produce vacancies and, eventually, structural modulations to recover a stable framework structure. In addition, the quality of high-resolution images is superior in crystals prepared by ultramicrotomy than by ion-milling, i.e., the anelastic scattering due to aperiodic matter is much higher in the latter case. However, this matter still needs further study. Contrary to what happens in large crystals, it is well known that in small crystals such as those obtained either with crushing or ultramicrotomy, any tension accumulated in the lattice due to structural deformation or modulation can be dissipated because of the greater proportion of unconstrained surfaces where tensions can be released (Zhang et al. 2002).

In any case, the possibility that the observed incommensurate modulation could be a primary feature cannot be completely ruled out. Indeed, the single-crystal synchrotron experiments may have not revealed the incommensurate modulation as the interaction constant of X-rays with the matter is generally about four orders of magnitude smaller than that for electrons.

In addition, the crystals used for single-crystal XRD are not the same used for TEM. Assuming that the observed structural modulation is a primary feature, from a theoretical point of view, it could be related either to a cation ordering over the metal sites, or to the presence of vacancies. The structure of heyrovskýite consists of five crystallographically distinct cation positions, Me1, Me2, Me3, Me4, and Me5. The Me2, Me3, Me4, and Me5 sites, which form octahedral chains running diagonally across the  $\text{PbS}$ -like layers, with distorted octahedral coordination (Fig. 1). The Me1 site, which displays a bicapped trigonal-prismatic coordination, is situated in a special position at the mirror plane that connects adjacent mirror-related, galena-type layers. Recent structural investigations on Ag-free heyrovskýite from Vulcano (Balić-Žunić et al. 2007; Pinto et al. in review) showed that the octahedral sites Me2 and Me3 located in the central zone of  $\text{PbS}$ -like slabs are pure Pb sites, as is Me1, whereas those closer to the boundary of  $(311)_{\text{PbS}}$  planes, i.e., Me4 and Me5, are mixed (Pb,Bi) sites, with almost equal occupancies. If the observed modulation is indeed a primary feature, the presence of cation sites with mixed (Pb,Bi) occupancy would suggest that it could arise from a Pb-Bi ordered distribution over Me4 and Me5 sites. The fact that no incommensurate modulations were observed in previous studies on LHS sulfosalts may be explained by the presence of small amounts of monovalent cations, such as Ag and/or Cu (Makovicky et al. 1991; Takéuchi and Takagi 1974), which stabilize sulfosalts structures (Makovicky 1977; Makovicky and Karup-Møller 1977a, 1977b) and promote polytypic disorder in the LHS.

Alternatively, the observed modulation could be triggered by the ordering of vacancies, naturally present in the samples or induced by ion-milling. This explanation applies equally well to both possible origins for the incommensurate modulation, i.e., as a primary feature or ion-beam induced artifact. The presence of vacancies associated with the substitution  $3\text{Pb}^{2+} \rightarrow 2\text{Bi}^{3+} + \square$  was first proposed by Takéuchi and Takagi (1974) in the pure synthetic heyrovskýite  $\text{Pb}_{6-x}\text{Bi}_{2+2x/3}\text{S}_9$ , and, recently, structure refinement of an Ag-free heyrovskýite crystal from Vulcano showed the occurrence of vacancies in the sole Me3 site (Balić-Žunić et al. 2007; Pinto et al. in review). On the other hand, if the presence of vacancies is related to the sublimation

of  $\text{Bi}_2\text{S}_3$ , the affected sites should be Me4 and Me5, the same sites involved in any Pb/Bi ordering. Curiously, these sites define planes whose normal makes an angle with  $\mathbf{b}^*$  of  $\sim 29^\circ$ , the same angle that the satellite reflections form with it (Fig. 1). These planes contain all the polyhedral sites (Me1 to Me5), parallel to the direction along which  $N$  is counted, and correspond closely (but not exactly, since polyhedral positions are slightly waved) to (140), whose interplanar distance is  $\sim 6.8 \text{ \AA}$ . Since the measured incommensurate modulation is  $\sim 75 \text{ \AA}$ , ordering of vacancies or of Pb-Bi cations should repeat the same scheme every eleven of such planes.

It is noteworthy that incommensurate modulation occurs only in Ag-free heyrovskýite but not in Ag-free lillianite, notwithstanding the similarities of the two phases and their occurrence in the same specimen. This disparity may be ascribed to their structural differences; lillianite differs from heyrovskýite in terms of the width of  $\text{PbS}$ -like slabs and  $\text{PbS}/\text{Bi}_2\text{S}_3$  ratio (3:1 and 6:1, respectively). Recent single-crystal XRD studies show that in Ag-free lillianite, Pb and Bi are statistically distributed among the sole Me1 and Me2 sites, with almost the same occupancy, while Me3 is completely filled by Pb (Pinto et al. 2006). Therefore, the different behaviors between Ag-free lillianite and heyrovskýite could be due to differences in the width of galena-like slabs or in the distribution of Pb and Bi within the slabs. Accordingly, Aizawa et al. (1983) found that the relative stability of LHS phases is related to the elastic strain energy arising at twin plane interfaces, and that a small change in Pb and Bi distribution greatly affects this energy, thus influencing sulfosal stability. Moreover, they noted that, depending on the cation distribution, the elastic strain energy could decrease or increase as the width of the slabs increases. This argument may also be valid when cation proportions are altered in a post-crystallization perturbation event, i.e., ion-beam irradiation during TEM specimen preparation.

#### ACKNOWLEDGMENTS

The authors are grateful to Allan Pring, University of South Australia, Gustaf Van Tendeloo and Oleg I. Lebedev of EMAT, University of Antwerp, Belgium, and an anonymous reviewer for their comments and suggestions, which greatly contributed to improve this research. We would like to thank also the associate editor, Hongwu Xu, for his help in handling the paper. This research is part of a Ph.D. study by D. Mitolo. Financial support was provided by MIUR (Ministero dell'Istruzione, dell'Università e Ricerca, Italy), University of Bari (Fondi Ateneo, ex 60% 2007), and by PRIN 2008, project "Sublimates and fumarolic encrustations (sulfosalts, halogen-sulfides, sulfates): crystal chemistry and genetic implications."

#### REFERENCES CITED

- Aizawa, K., Iguchi, E., and Tilley, R.J.D. (1983) The elastic strain energy stability of some idealized lead-bismuth sulfides. *Journal of Solid State Chemistry*, 48, 284–294.
- Akizuki, M. (1981) Investigation of phase transition of natural ZnS minerals by high resolution electron microscopy. *American Mineralogist*, 66, 1006–1012.
- (1983) Investigation of phase transition of natural ZnS minerals by high resolution electron microscopy: Reply. *American Mineralogist*, 68, 847–848.
- Amouric, M. and Baronnet, A. (1983) Effect of early nucleation conditions on synthetic muscovite polytypism as seen by high resolution transmission electron microscopy. *Physics and Chemistry of Minerals*, 9, 146–159.
- Barber, D.J. (1970) Thin foils of non-metals made for electron microscopy by sputter etching. *Journal of Materials Science*, 5, 1–8.
- Balić-Zunić, T., Garavelli, A., Pinto, D., and Vurro, F. (2007) Structural investigation on the Ag-free heyrovskýite from Vulcano (Aeolian Island, Southern Italy). VI FIST-Geotitalia, Rimini (Italy), 12–14/09/2007.
- Borodaev, Y.S., Garavelli, A., Garbarino, C., Grillo, S.M., Mozgova, N.N., Uspenskaya, T.Y., and Vurro, F. (2001) Rare sulfosalts from Vulcano, Aeolian Islands, Italy. IV. Lillianite. *Canadian Mineralogist*, 39, 1203–1215.
- Borodaev, Y.S., Garavelli, A., Garbarino, C., Grillo, S.M., Mozgova, N.N., Paar, W.H., Topa, D., and Vurro, F. (2003) Rare sulfosalts from Vulcano, Aeolian Islands, Italy. V. Selenian heyrovskýite. *Canadian Mineralogist*, 41, 429–440.
- Ciobanu, C.L., Pring, A., and Cook, N.J. (2004) Micron- to nano-scale intergrowths among members of the cuprobismutite series and padraite: HRTEM and microanalytical evidence. *Mineralogical Magazine*, 68, 279–300.
- Ferraris, G., Makovicky, E., and Merlini, S. (2004) Crystallography of modular materials. *IUCr Monographs on Crystallography*, 15, p. 1–370. Oxford, U.K.
- Hovmöller, S. (1992) CRISP: crystallographic image processing on a personal computer. *Ultramicroscopy*, 41, 121–135.
- Kilaas, R. (1998) Optimal and near-optimal filters in high-resolution electron microscopy. *Journal of Microscopy*, 190, 45–51.
- Kissin, S.A. and Owens, D.R. (1986) The properties and modulated structure of potosiite from the Cassiar District, British Columbia. *Canadian Mineralogist*, 24, 45–50.
- Loginov, Yu. Yu. and Brown, P.D. (1992) 100 keV electron beam induced decomposition of II-VI compounds. *Physica Status Solidi (a)*, 132, 323–337.
- Madelung, O., Rössler, U., and Schulz, M. (1998a) Bismuth sulfide ( $\text{Bi}_2\text{S}_3$ ): Heat capacity, density, melting point. In E. Landolt-Börnstein, Eds., *Non-tetrahedrally bonded elements and binary compounds I*, 41C, p. 942. Springer, Berlin.
- (1998b) Lead sulfide (PbS): Debye temperature, heat capacity, density, melting point. In E. Landolt-Börnstein, Eds., *Non-tetrahedrally bonded elements and binary compounds I*, 41C, p. 876. Springer, Berlin.
- Makovicky, E. (1977) Chemistry and crystallography of the lillianite homologous series. III. Crystal chemistry of lillianite homologues. Related phases. *Neues Jahrbuch für Mineralogie Abhandlungen*, 131, 187–207.
- Makovicky, E. and Karup-Møller, S. (1977a) Chemistry and crystallography of the lillianite homologous series. I. General properties and definition. *Neues Jahrbuch für Mineralogie Abhandlungen*, 130, 264–287.
- (1977b) Chemistry and crystallography of the lillianite homologous series. II. Definition of new minerals: Eskimoite, vikingite, ourayite, and treasurerite. Redefinition of schirmerite and new data on the lillianite-gustavite solid solution series. *Neues Jahrbuch für Mineralogie Abhandlungen*, 131, 56–82.
- Makovicky, E., Mumme, W.G., and Hoskins, B.F. (1991) The crystal structure of Ag-Bi-bearing heyrovskýite. *Canadian Mineralogist*, 29, 553–559.
- Malis, T.F. and Steele, D. (1990) Ultramicrotomy for materials science. *Materials Research Society Symposium Proceedings*, 199, 3–42.
- Mitchell, D.R.G. (2007) HRTEM filter. Digital Micrograph Script Database. [http://www.felmizfe.tugraz.at/dm\\_scripts/dmscript1.html](http://www.felmizfe.tugraz.at/dm_scripts/dmscript1.html).
- Mitolo, D. (2008) Structural study of Pb-Bi sulfosalts from Vulcano (Aeolian Island, Italy) by Transmission Electron Microscopy. Ph.D. Thesis (XXI Ciclo, 2005–2008), Dip. Geomineralogico, Università degli Studi di Bari, 1–90.
- Pierce, L. and Buseck, P.R. (1978) Superstructuring in the bornite-digenite series: A high-resolution electron microscopy study. *American Mineralogist*, 63, 1–16.
- Pinto, D. (2004) Mineralogy, crystal chemistry and structures of sulfosalts from Vulcano (Aeolian Islands, Italy): Ag-free lillianite, Cl-bearing galenobismutite, kirkiite, and the new mineral vurroite. Ph.D. Thesis (XVII Ciclo, 2001–2004), Dip. Geomineralogico, Università degli Studi di Bari, 1–165.
- Pinto, D., Balić-Zunić, T., Garavelli, A., Makovicky, E., and Vurro, F. (2006) Comparative crystal structure study of Ag-free lillianite and galenobismutite from Vulcano (Aeolian Islands, Italy). *Canadian Mineralogist*, 44, 159–175.
- Price, G.D. and Yeomans, J. (1984) The application of the ANNNI model to polytypic behaviour. *Acta Crystallographica*, B40, 448–454.
- Pring, A. (1989) Structural disorder in the aikinite and krupkaite. *American Mineralogist*, 74, 250–255.
- (1990) Disorder intergrowths in lead-arsenic sulfide minerals and the paragenesis of the sartorite-group minerals. *American Mineralogist*, 75, 289–294.
- (1995) Annealing of synthetic hammarite,  $\text{Cu}_2\text{Pb}_2\text{Bi}_4\text{S}_8$ , and the nature of cation-ordering processes in the bismuthinite-aikinite series. *American Mineralogist*, 80, 1166–1173.
- (2001) The crystal chemistry of the sartorite group minerals from Lenggenbach, Binntal, Switzerland: a HRTEM study. *Schweizerische Mineralogische und Petrographische Mitteilungen*, 81, 69–87.
- Pring, A. and Ciobanu, C.L. (2007) Chemical modulations in Pb-Bi sulfosalts: A glimpse at minerals in solid-state chemistry. In K.D.M. Harris and P.P. Edwards, Eds., *Turning points in solid-state, materials and surface science*, p. 239–249. RSC Publishing Book, London.
- Pring, A. and Etschmann, B. (2002) HRTEM observations of structural and chemical modulations in cosalite and its relationship to the lillianite homologues. *Mineralogical Magazine*, 66, 451–458.
- Pring, A. and Graeser, S. (1994) Polytypism in baumhauerite. *American Mineralogist*, 79, 302–307.
- Pring, A. and Hyde, B.G. (1987) Structural disorder in lindstromite: A bismuthinite-aikinite derivative. *Canadian Mineralogist*, 25, 393–399.
- Pring, A., Williams, T., and Withers, R. (1993) Structural modulation in sartorite: An electron microscope study. *American Mineralogist*, 78, 619–626.
- Pring, A., Jercher, M., and Makovicky, E. (1999) Disorder and compositional

- variation in the lillianite homologous series. *Mineralogical Magazine*, 63, 917–926.
- Prodan, A., Bakker, M., Versteegh, M., and Hyde, B.G. (1982) A microscopic study of synthetic PbS-rich homologues  $n\text{PbS}\cdot m\text{Bi}_2\text{S}_3$ . *Physics and Chemistry of Minerals*, 8, 188–192.
- Skowron, A. and Tilley, R.J.D. (1986) The transformation of chemically twinned phases in the PbS-Bi<sub>2</sub>S<sub>3</sub> system to the galena structure. *Chemica Scripta*, 26, 353–358.
- (1990) Chemically twinned phases in the Ag<sub>2</sub>S-PbS-Bi<sub>2</sub>S<sub>3</sub> system. Part I: Electron microscope study. *Journal of Solid State Chemistry*, 85, 235–250.
- Spurr, A.R. (1969) A low-viscosity epoxy resin embedding medium for electron microscopy. *Journal of Ultrastructural Research*, 26, 31–43.
- Takagi, J. and Takéuchi, Y. (1972) The crystal structure of lillianite. *Acta Crystallographica*, B28, 649–651.
- Takéuchi, Y. and Takagi, J. (1974) The structure of heyrovskýite ( $6\text{PbS}\cdot\text{Bi}_2\text{S}_3$ ). *Proceedings of the Japan Academy*, 50, 76–79.
- Tilley, R.J.D. and Wright, A.C. (1982) Chemical twinning in the PbS region of the PbS-Bi<sub>2</sub>S<sub>3</sub> system. *Chemica Scripta*, 19, 18–22.
- Vurro, F., Garavelli, A., Garbarino, C., Mošlo, Y., and Borodaev, Y.S. (1999) Rare sulfosalts from Vulcano, Aeolian Islands, Italy. II. Mozgovaites  $\text{PbBi}_4(\text{S},\text{Se})_n$ , a new mineral species. *Canadian Mineralogist*, 37, 1499–1506.
- Williams, D.B. and Carter, C.B. (1996) *Transmission Electron Microscopy, A Textbook for Materials Science*, 729 p. Plenum Press, New York.
- Williams, T.B. and Hyde, B.G. (1988) Electron microscopy of cylindrite and franckeite. *Physics and Chemistry of Minerals*, 15, 521–544.
- Williams, T.B. and Pring, A. (1988) Structure of lengenbachite: A high-resolution transmission electron microscope study. *American Mineralogist*, 73, 1426–1433.
- Zhang, F., Chan, S.W., Spanier, J.E., Apak, E., Jin, Q., Robinson, R.D., and Herman, I.P. (2002) Cerium oxide nanoparticles: Size-selective formation and structure analysis. *Applied Physics Letters*, 80, 127–129.

MANUSCRIPT RECEIVED FEBRUARY 12, 2010

MANUSCRIPT ACCEPTED SEPTEMBER 6, 2010

MANUSCRIPT HANDLED BY HONGWU XU